Proceedings of the ASME 2010 3rd Joint US-European Fluids Engineering Summer Meeting and 8th International Conference on Nanochannels, Microchannels, and Minichannels
FEDSM-ICNMM2010
August 1-5, 2010, Montreal, Canada

FEDSM-ICNMM2010-30473

PARAMETER OPTIMIZATION OF A MICRO HEAT SINK WITH CIRCULAR PIN-FINS

Mustafa Koz
Sabanci University, Faculty of Engineering and Natural Sciences
Istanbul, Turkey

Ali Kosar
Sabanci University, Faculty of Engineering and Natural Sciences
Istanbul, Turkey

ABSTRACT

Micro heat sinks have a broad applicability in many fields such as aerospace applications, micro turbine cooling, micro reactors, electronics cooling and micro biological applications. Among different types of micro heat sinks, those with micro pin-fins are becoming popular due to their enhanced heat removal performance. However, relevant experimental data is still scarce, and few optimization studies are present in the literature.

In order to effectively optimize their performance, an extensive parametric study is necessary and should be based on a realistic model. Moreover, micro pin fin heat sinks should be optimized according to appropriate performance criteria depending on the application. The objective of this paper is to fill the research gap in micro pin fin heat sink optimization based on realistic configurations.

In this paper, the parameters for micro pin optimization are the pin-fin height over diameter ratio ($0.5<H/D<5$) and the longitudinal and transverse pitch ratios ($1.5<(SL,ST)/D<5$), while Reynolds number and heat flux provided from the base of the micro heat sink are in the range of ($1<\mathrm{Re}<100$) and ($20<q(\mathrm{W/cm^2})<500$), respectively.

In this research, micro pin fin heat sinks are three dimensionally modeled on a one-to-one scale with the use of commercially available software COMSOL Multiphysics 3.5a. Full Navier-Stokes equations subjected to continuity and energy equations are solved for stationary conditions. To have increased computational efficiency, half of the heat sink is modeled with the use of a symmetry plane. In order to validate the use of numerical models, parametric values from previous experimental data available in the literature are exactly taken and simulated. The numerical and experimental results show a good agreement. After this validation, optimization study is performed using the three dimensional, numerical models.

NOMENCLATURE

2D	Two Dimensional
3D	Three Dimensional
A	Area
C	Heat Capacity
D	Fin Diameter
H	Fin and micro channel height
L	Fluid domain length
P	Pressure
Re	Reynolds number
ST	Transverse distance between pin-fins
SL	Longitudinal distance between pin-fins
T	Temperature
W	Width of the fluid domain
f	Friction factor
h	Heat transfer coefficient
k	Conductivity
$\mathbf{n}$	Normal vector to a surface
q	Heat flux
$\mathbf{q}$	Heat flux vector
r	Radius of pin-fin
$\mathbf{u}$	Velocity vector of the fluid
u, v, w	Velocity components of the fluid
$\boldsymbol{x}$	Spatial coordinate vector
x, y, z	Spatial coordinates

Greek Letters

η	Dynamic viscosity
ρ	Mass density

Subscript

amb	Ambient
c	Cross sectional
fin	Fin
hb	Heated base
hs	Heated surfaces
in	Inlet related
max	Maximum
out	Outlet related
sur	Surface related

1 INTRODUCTION

Microelectronic devices dissipate more heat as they decrease in size. As a response to this challenging heat removal demand, parallel micro channels were initially utilized and received considerable attention [1-9]. They are now ready to be elaborated to more complex structures with the help of recent advancements in micro fabrication techniques [10, 11].

The latest and most widely used micro heat removing devices are the micro heat sinks with circular pin-fins. These devices consist of a micro channel with an array of either staggered or aligned circular micro pin-fins. The circular pin-fins have the same height (H) as the micro channel, and their diameters' (D) subjectivity to change leads to a varying height to diameter ratio (H/D) (typically between 0.5 and 5). Moreover, there is an option of using various coolant fluids, for which water is mostly preferred. In this paper, the pin-fins are in staggered configuration, and water is the coolant fluid under single-phase flow conditions. The comparison between micro channel and micro pin-fin heat sinks indicates that the latter provides a larger heat transfer area per volume in addition to higher heat transfer coefficients due to boundary layer disruption and mixing effects [12,13].

The current literature covers micro pin fin heat sinks' hydrodynamic and thermal characteristics and gives valuable information about this subject [12-23]. Most of these previous studies utilize experimental data to compare them to existing conventional correlations for predicting Nusselt numbers or friction factors of micro pin-fin heat sinks. However, there are only few numerical studies for accurately simulating heat and fluid flow in micro pin-fin heat sinks. This work aims at filling the gap of an extensive numerical study in this subject in addition to providing valuable insight into optimization of micro pin fin heat sinks.

2 METHODOLOGY

The height over diameter ratio (H/D) of the pin-fin is changed from 0.5 to 5, while the height of the pin-fin is kept constant and equal to the micro channel height (for validation runs: 243 μm, for parametric runs: 250 μm). The longitudinal and transverse distance(s) to diameter ratios (SL/D,ST/D) are between 1.5 and 5. Lastly, the Reynolds number ranges from 20 to 100. These parameters (H/D, SL/D and ST/D) are chosen according to the most frequently used values in the available literature [12-23]. Moreover, the rationale for the Reynolds number range is twofold: to address to scant data in the literature regarding the very low Reynolds numbers as well as to decrease the possibility of transition to a turbulent flow in micro pin-fin heat sinks.

In order to validate the results of parametric models, a one-to-one validation model of a micro pin-fin heat sink from the work of Kosar and Peles [20] is simulated. Throughout this work, all procedures will be explained for two cases: the validation model and the parametric model. The procedures for these two different types of models may intersect at some points and will be elaborated in the following sections.

2.1 Drawing

Parametric models do not fully encompass a whole micro channel and its micro pin-fins. Instead, to better and faster simulate the heat and fluid flow across micro pin fins, a geometrically repetitive pattern in a real micro heat sink is cut and simulated individually. The 2D-3D representations of a repetitive pattern, which consists of four micro pin-fins, and a symmetry plane are depicted in Figs. 1 and 2.

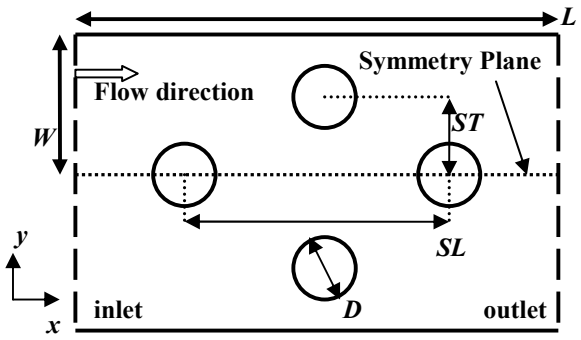

Figure 1: Cross section of a typical micro pin-fin heat sink model

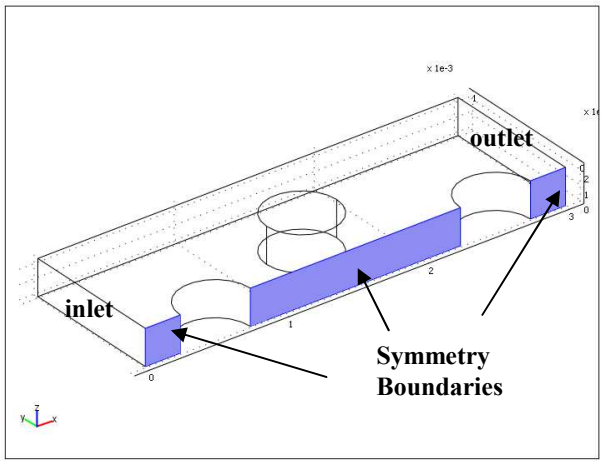

Figure 2: Symmetry boundaries of a typical, 3D micro pin-fin heat sink model.

Half of the domain above is simulated by using the symmetry plane. The upper half domain in Fig. 1 always consists of two halves and a whole micro pin-fin, and the pin-fins are drawn as extruded cuts from the fluid domain to define the solid-to-fluid heat transfer boundaries.

In order to have the same number of pin-fins in each case; varying D, SL and ST values redefine the dimensions of the fluid domain dimensions. The dimensions (WxL) of the fluid domain are expressed as:

$$W = \frac{ST}{2} + 2r \quad (1)$$

$$L = 2SL + 4r \quad (2)$$

SL and *ST* are functions of *D*, which has varying values presented in Table 1.

***H*(μm)**	**250**
H*/*D	**0.5, 1, 2, 4, 5**
***D* (μm)**	**500, 250, 125, 62.5, 50**
SL*/*D*, *ST*/*D	**1.5, 2, 5**

Table1: Geometric parameters of parametric models.

For each pin-fin diameter value (*D*), *SL* and *ST* parameter sets are formed and a separate model is simulated. In order to show the effects *SL*/*D* and *ST*/*D* parameters separately, a reference case is chosen (*SL*/*D* and *ST*/*D* are 2) and variations are simulated in one parameter at a time as presented in Table 2.

	SL*/*D			
		1.5	2	5
ST*/*D	1.5			
	2			
	5			

Table2: A sample *SL*-*ST*/*D* combination of parameters.

The validation micro pin-fin heat sink model is based on the 2CLD device experimentally observed in the work of Kosar and Peles [20]. The device has dimensions of (*W*x*L*x*H*) 1800x10000x243 μm. To exploit the symmetry boundary conditions, half of the channel width (900 μm) is used. The micro pin-fins are 100 μm in diameter and *SL*-*ST* values are 350-150 μm, respectively.

2.2 Fluid Flow

Due to the varying temperature of the fluid throughout the micro channel, flows in all models are governed by weakly compressible, stationary Navier-Stokes equations. Therefore, the physical properties of water, such as mass density (ρ) and dynamic viscosity (η), are all subjected to change because of the varying temperature. Navier-Stokes equations are subject to a fully compressible formulation of continuity:

$$\frac{\partial \rho}{\partial t} + \nabla \cdot (\rho \mathbf{u}) = 0 \tag{3}$$

$$\rho \mathbf{u} \cdot \nabla \mathbf{u} = \ldots$$

$$\ldots = -\nabla p + \nabla \cdot \left(\eta \left(\nabla \mathbf{u} + (\nabla \mathbf{u})^T \right) - \frac{2}{3} \eta (\nabla \mathbf{u}) \mathbf{I} \right) + \mathbf{F} \tag{4}$$

The boundary condition at the inlet of a parametric model is a variable inlet velocity (u_{in}):

$$\mathbf{u} \cdot \mathbf{n} \Big|_{\mathbf{x}=0,y,z} = u_{in} \tag{5}$$

u_{in} is set according to the desired local Reynolds number across the pin fin:

$$\mathrm{Re} = \frac{\rho D u_{\max}}{\eta} \tag{6}$$

$$u_{\max} = \frac{W}{(W - D)} u_{in} \tag{7}$$

For all parametric models, the Reynolds numbers to be simulated are 20, 30, 40, 50, 60, 80, and 100. u_{in} is calculated using the following formula:

$$u_{in} = \frac{\mathrm{Re}\, \eta (W - D)}{D \rho W} \tag{8}$$

In the parametric model, the outlet is set be an open boundary with no normal stress:

$$\left[-P\mathbf{I} \right] \cdot \mathbf{n} \Big|_{\mathbf{x}=L,y,z} = 0 \tag{9}$$

In the validation model, the inlet and outlet are set to have non-zero pressure for a pressure differential along the channel:

$$\left[-P\mathbf{I} \right] \cdot \mathbf{n} \Big|_{\mathbf{x}=0,y,z} = P_{in} \tag{10}$$

$$\left[-P\mathbf{I} \right] \cdot \mathbf{n} \Big|_{\mathbf{x}=L,y,z} = P_{out} \tag{11}$$

$$P_{in} > P_{out} \tag{12}$$

Symmetry boundary condition is set for one side of the channel as in Fig. 2. The symmetry plane cuts the micro channel and the pin-fins located at the middle of channel width.

All other boundaries are set as no-slip boundary conditions.

2.3 Heat Transfer

For all the models, steady state conditions are imposed. All properties of water, such as mass density (ρ), dynamic viscosity (η), heat capacity (C) and conductivity (k), are temperature dependent. The governing energy equation becomes:

$$\rho C (\mathbf{u} \cdot \nabla) T = -(\nabla \cdot q) = \nabla \cdot (k \nabla T) \tag{13}$$

In real life practices, a prescribed heat flux (q_{hb}) is applied at the base of the micro channel (A_{hb}) with an area of *W*x*L*. However, in this numerical work, the heat flux is homogenously distributed (q_{in}) to the whole heated surfaces (A_{hs}: base without the cross sectional area of pin-fins and with pin-fin surfaces) as in Fig. 3.

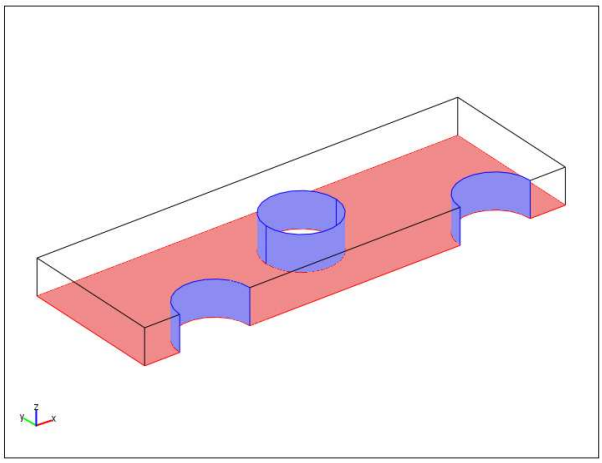

Figure 3: Heated surfaces of the micro pin-fin heat sink

Therefore, the ratio of the heat flux at the heated base and at the whole fluid interacting surfaces is:

$$q_{in} = q_{hb}\frac{A_{hb}}{A_{hs}} = q_{hb}\frac{WL}{WL + 2\left(A_{f,sur} - A_{f,c}\right)} \qquad (14)$$

Additionally, the inlet temperature (T_{in}) is constant and set to 300 K for parametric models while it was varied for the validation model according to experimental conditions:

$$T\Big|_{\mathbf{x}=0,y,z} = T_{in} \qquad (14)$$

The channel outlet is set to have outward convective flux:

$$\mathbf{q}\cdot\mathbf{n}\Big|_{\mathbf{x}=L,y,z} = \rho C T\mathbf{u}\cdot\mathbf{n}\Big|_{\mathbf{x}=L,y,z} \qquad (15)$$

All other boundaries are set as thermally isolated boundaries.

2.3 Mesh and Solver Settings

The simulation package, COMSOL Multi physics 3.5a is used and its Weakly Compressible Navier-Stokes and Convection-Conduction modules are integrated to the model presented above. This software is synchronized with Solid Works 2008 SP2.1 to perform geometric sweeps.

This software runs in a work station with an Intel Xeon 3.0GHz processor with 32GB RAM. The server's operating system is Microsoft XP 64bit edition.

The micro pin-fins surfaces, the heated base and the fluid sub domain were meshed with a maximum element size of *r*/2. Mesh elements on the surfaces and volumes are triangular and tetrahedral, respectively. Total mesh element amount can vary from 10000 to 50000 according the changing aspect ratios of the parametric models since the models with higher *H/D* ratio demand a greater number of mesh elements. The mesh independency check for *D*=500 geometry reveals that the mesh configuration with maximum element size equals to *r*/2, providing a mesh independency less than 1%.

Mesh element size	*r*	*r/1.5*	*r*/2
ΔT heated surfaces	40.06	40.652	40.424

Table3: Mesh independency check for *D*=500 geometry

To solve the governing equations, Parallel Direct Sparse Solver (PARDISO) runs separately for segregated parameters (fluid flow and heat transfer variables). The absolute tolerance is set to be 10^{-3}. The simulations can take from10 minutes to 60 minutes.

2.4 Post Processing of the Results

For the validation model, the pressure difference between the inlet and the outlet is given, and the resulting flow velocity is compared to the experimental results of Kosar and Peles [20].

In parametric models, additional channel walls are introduced to encircle a repetitive pin-fin pattern. However, in the validation model, each repetitive pattern is not separated by no-slip walls. These encircling no-slip walls in the parametric models introduce additional pressure losses. In order to accurately evaluate the pressure loss that pin-fins introduce in a parametric model, total force in the *x* direction (F_x) is integrated over pin-fin surfaces, then surface averaged and substituted for channel pressure difference.

$$\Delta P = \frac{\int_{\text{Fin surfaces}} F_x dA}{A_{fin,sur}} \qquad (16)$$

Friction factor for each pin-fin is expressed for N_{row}=2.

$$f_{fin} = \frac{2\Delta P_{fin}}{N_{row}\rho u_{\max}^2} = \frac{\Delta P_{fin}}{\rho u_{\max}^2} \qquad (17)$$

In order to evaluate the heat transfer performance of the models, the outlet and heated base temperatures need to be calculated:

$$T_{out} = \frac{\int_{\substack{\text{outlet}\\ \text{surface}}} TdA}{A_{out}} \qquad (18)$$

$$T_{hb} = \frac{\int_{\substack{\text{heated}\\ \text{surface}}} TdA}{WL + 2\left(A_{fin,sur} - A_{fin,c}\right)} \qquad (19)$$

By using Eq. 20 and 21, average heat transfer coefficients, Nusselt numbers, and fin efficiencies are calculated iteratively and in similar lines as previous experimental studies in the literature [18, 20, 21]:

$$T_{amb} = \frac{T_{in} + T_{out}}{2} \tag{20}$$

$$h = \frac{q_{hb} WL}{\left(N_{fin}\left(\eta_{fin} A_{fin} - A_{c,fin}\right) + WL\right)\left[T_{hb} - T_{amb}\right]} \tag{21}$$

$$\eta_{fin} = \frac{\tanh\left(m_{fin} H\right)}{m_{fin} H} \tag{22}$$

$$m_{fin} = \sqrt{\frac{hA_{fin}}{Hk_{fin} A_{fin,c}}} \tag{23}$$

3 RESULTS

3.1 Validation Runs

The 2CLD micro pin-fin heat sink device from the experiments of Kosar and Peles [20] is exactly modeled for validation purposes. The simulation results show a very strong agreement with the experimental data. Experimental applied pressure difference (ΔP) and heat flux (q) are taken as the input parameters.

At a given pressure difference, the numerically calculated average flow velocities across the channel are more than 99% accurate compared to those achieved in the experimental work.

Figure 4 depicts the temperature distribution along and at the mid height of the channel. The minimum and maximum temperatures are represented by dark blue and red colors, respectively. The left side wall of the micro channel has an increasing temperature (which finally reaches a global maximum), as it gets closer to the outlet.

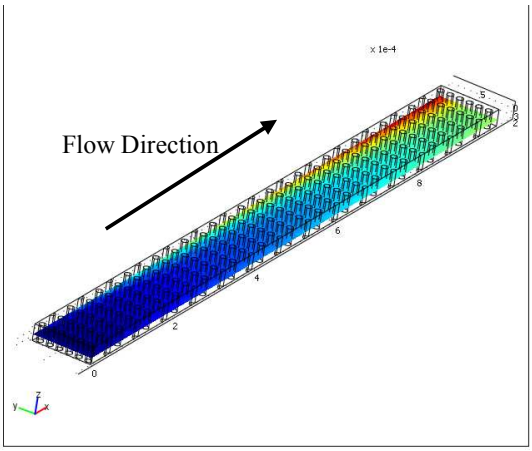

Figure 4: Temperature distribution numeric model of 2CLD device from the experiments of Kosar and Peles [20].

In order to show the agreement between the validation model and experimental results, the surface averaged heated base temperatures are plotted against applied heat fluxes for two fixed pressure drops. Figure 5 proves the strong agreement between numerical and experimental results for increasing pressure differentials. The corresponding maximum error percentages (between experimental and numerical surface temperatures) for ΔP=36.8 and 20.3 kPa are 13% and 7%, respectively.

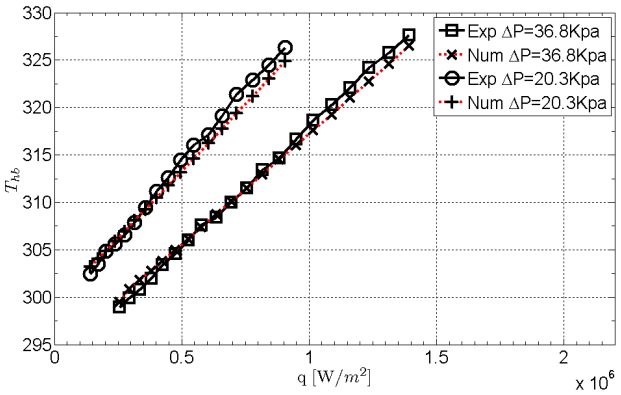

Figure 5: Numerical vs experimental surface averaged temperatures for the heated base of the micro channel in cases of varying pressure differentials.

3.2 Parametric Runs

The parametric runs reveal the performance of various pin-fin configurations surrounded by channel walls with varying *ST*-*SL* values under various flow conditions. It should be noted that the number of pin-fins in a configuration is kept constant in the fluid domain with varying dimensions. Thus, the denser pin-fin spacing does not necessarily lead to higher Nusselt numbers or friction factors. An example can be given for a case of pin-fins with 500μm diameter at Re=100. In this case, the *SL*/*D* remains constant while *ST*/*D* is varied from 1.5 to 5. The increase in *ST* increases the channel width due to the constant pin fin number per fluid domain imposed in this study. Therefore, the required average inlet velocity for the same Reynolds number (100) is increased from 0.0857 to 0.142 m/s. The convective heat flux profiles along the fluid domain are depicted at slices along the channel in Figs. 6 and 7. These slices are taken from the mid height of the channel, where fluid flow is least affected by no-slip boundary conditions. As the convective heat flux increases, the color on the slice makes a transition from blue to red. It can be seen that higher convective heat flux values occupy more area for *ST*/*D*=5 (Fig. 7), a condition, which leads to higher Nusselt numbers.

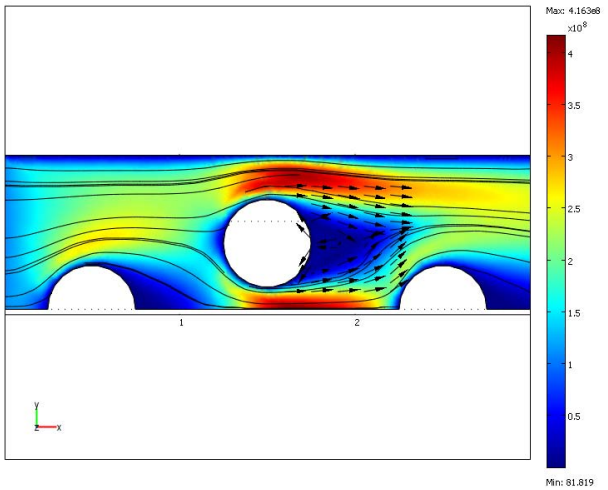

Figure 6: Convective flux slice, streamlines and velocity arrows for *D*=500, Re=100, *SL*/*D*=2, *ST*/*D*=1.5

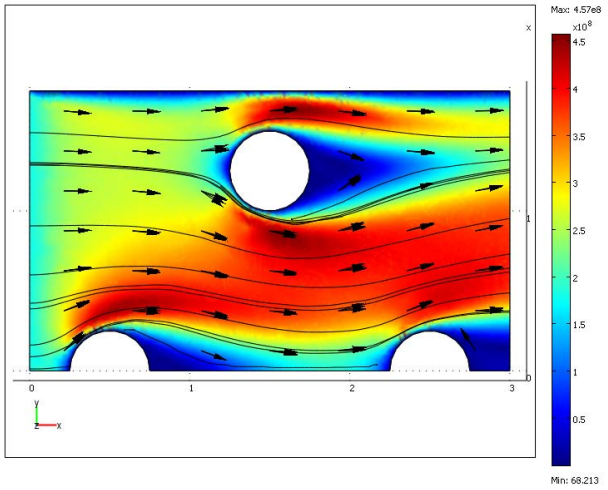

Figure7: Convective flux slice, streamlines and velocity arrows for *D*=500, Re=100, *SL*/*D*=2, *ST*/*D*=5

Figures 6 and 7 also show that an increased *ST* value allows more fluid to pass between the three heated pin-fins rather than the unheated channel wall. Moreover, in the configuration of *ST*/*D*=1.5, the streamlines show that three pin-fins stand as one single body against the fluid flow. However, the streamlines need to be reformed for each pin-fin at a greater ST/D ratio, a condition, which leads to a higher friction factor.

As opposed to the effect of *ST*/*D*, an increasing value of *SL*/*D* introduces lower friction factors and Nusselt numbers. As depicted in Figs. 8 and 9, increasing SL/D value allows the deformed flow streamlines to become more regular. The streamlines in *SL*/*D*=1.5 have a lower radius of curvature than *SL*/*D*=5. Moreover, the convective heat flux is more homogenously distributed among pin-fins in *SL*/*D* =1.5 than in *SL*/*D*=5.

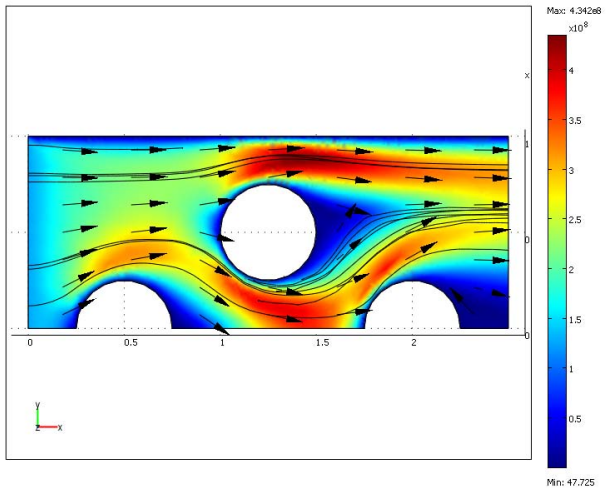

Figure 8: Convective flux slice, streamlines and velocity arrows for *D*=500, Re=100, *ST*/*D*=2, *SL*/*D*=1.5

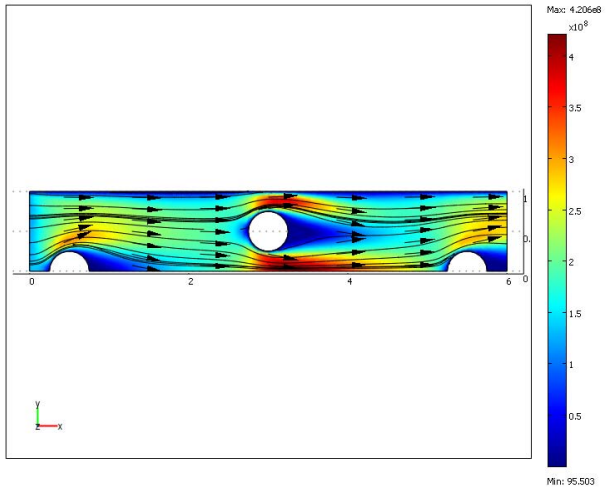

Figure 9: Convective flux slice, streamlines and velocity arrows for *D*=500, Re=100, *ST*/*D*=2, *SL*/*D*=5

In Figs. 10-14, friction factor versus Reynolds number profiles are depicted at a fixed *H*/*D* value with five different combinations of *ST*/*D*-*SL*/*D*. The major trend among all figures is the decrease of friction factors with an increase in *H*/*D*.

There is a strong relationship between the friction factor and *ST*/*D*. For each configuration, there are the same number of pin-fins, and thus, the same number of obstacles to the flow across. As the pin-fins move away from each other, they cannot stand as one body against the fluid flow and the streamlines are more distorted, which introduces additional friction. Moreover, as *ST*/*D* increases, the dependency of friction factor, *f*, on Re weakens.

In contrast to *ST*/*D*, *SL*/*D* has an adverse effect on friction factor. As *SL*/*D* increases, the flow is less affected by the geometric blockages of pin-fins, and pin-wake (downstream the pin fin) interactions become minor.

Among all combinations of *SL*/*D* and *ST*/*D*, the friction factor difference between the worst and best scenario can vary from 75% to 25%, as *H*/*D* increases. This shows that *SL*/*D* and *ST*/*D* ratios are more critical in lower *H*/*D* ratios.

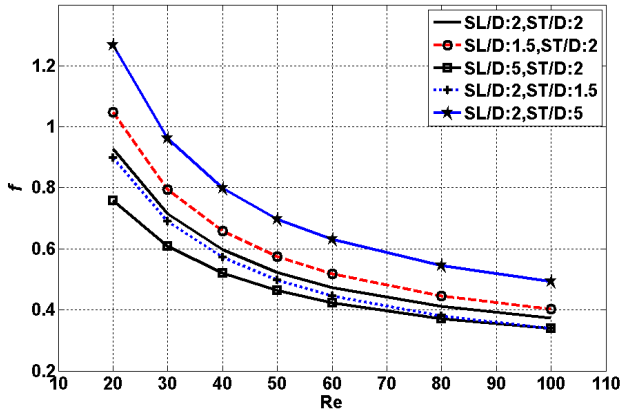

Figure 10: *f* vs Re for *H*/*D*=0.5

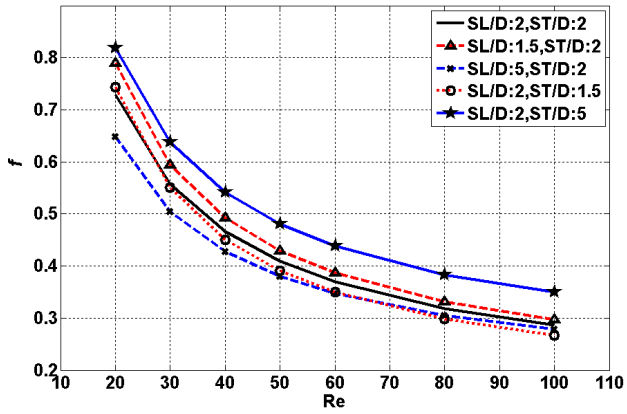

Figure 11: *f* vs Re for *H*/*D*=1

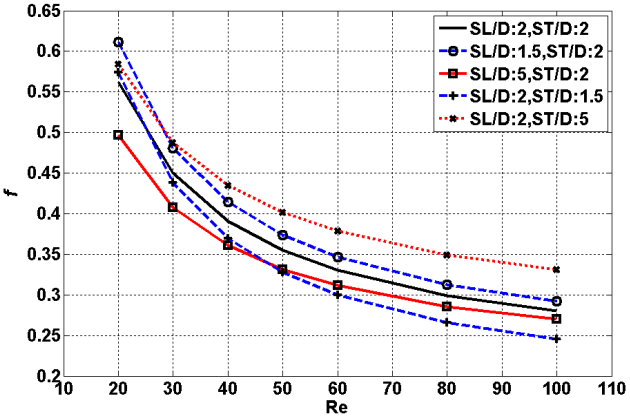

Figure 12: *f* vs Re for *H*/*D*=2

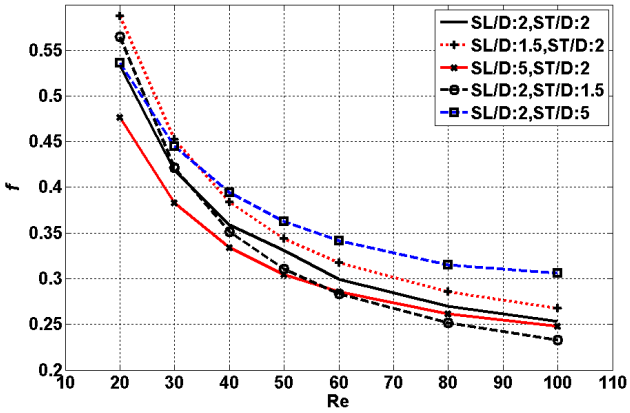

Figure 13: *f* vs Re for *H*/*D*=4

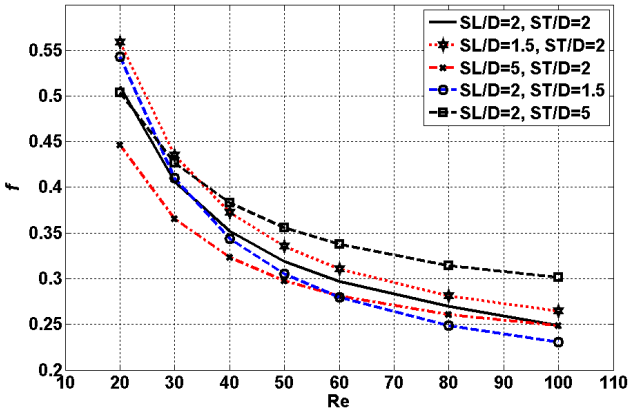

Figure 14: *f* vs Re for *H*/*D*=5

According to Figs. 15-18, the trend in Nusselt number with respect to the Reynolds number changes for the Reynolds numbers starting from 60 (for most cases) and differs from its trend at lower Reynolds numbers. Such a change in Nusselt number behavior was also previously reported and attributed to the formation of attached vortices by Kosar and Peles [20]. Moreover, as *H*/*D* increases, the effects of *SL*/*D* and *ST*/*D* weaken as in the friction factor case.

The effects of *SL*-*ST*/*D* for low *H*/*D* ratios on Nusselt numbers comply with their effect on friction factor. As depicted in Fig. 15 for *H*/*D*=0.5, the configuration resulting in higher friction factor leads to a higher Nusselt number. However, as *H*/*D* increases, the configurations start to have a more complex behavior.

In Figure 16, *ST*/*D*=1.5*SL*/*D=2* configuration has a lower Nusselt number than the reference case (*ST*-*SL*/*D*=2) for Reynolds numbers lower than 60. After Re=60, it outperforms the reference case. *ST*/*D*=5 *SL*/*D*=2 configuration results in lower Nusselt numbers than the reference case but it is more adversely affected by higher Re numbers. *SL*/*D* effect on Nu shows the same trend as in friction factor.

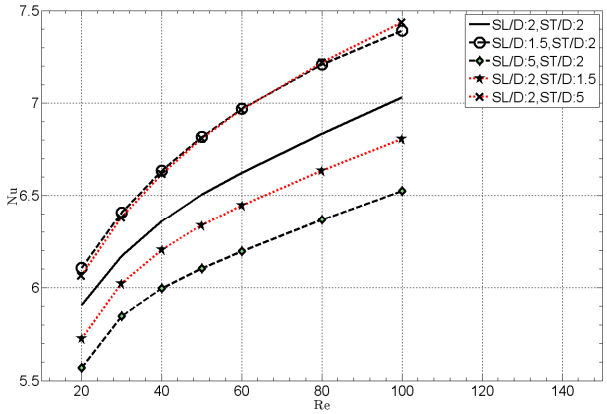

Figure 15: *H*/*D*=0.5, Nu vs Re

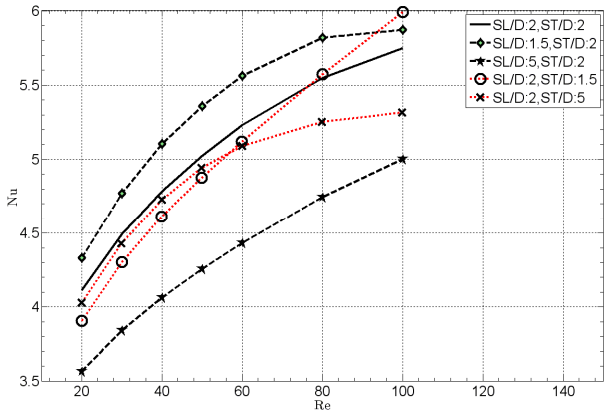

Figure 16: *H*/*D*=1, Nu vs Re

The trends in Nu become more complex with increasing *H/D* ratio. As shown in Figure 17, *ST*/*D*=5*SL*/*D*=2 configuration has higher Nu values compared to the reference case over the whole Re range. *SL*/*D*=1.5 *SL/D=2* configuration has highest Nusselt numbers at lower Re (Re<60) and is outperformed by *ST*/*D*=5*SL*/*D*=2 configuration.

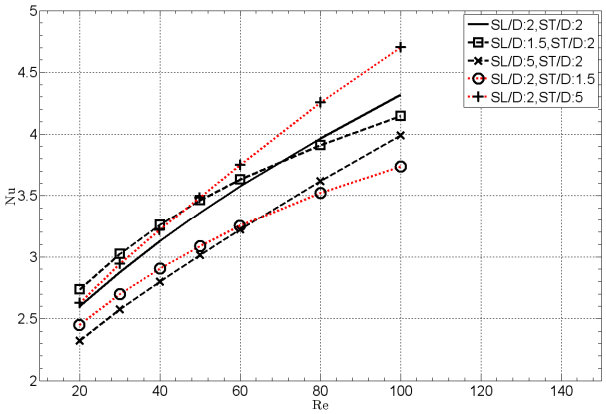

Figure 17: *H*/*D*=2, Nu vs Re

In Figure 18, all configurations seem to converge to the same Nusselt number at higher Re. For lower Reynolds numbers, *ST*/*D*=1.5 *SL*/*D*=2 configuration has a tendency to outperform all configurations. The decrease in Nu with increasing *H/D* is more evident in this *H/D* ratio. This could be associated with the decrease in fin efficiency.

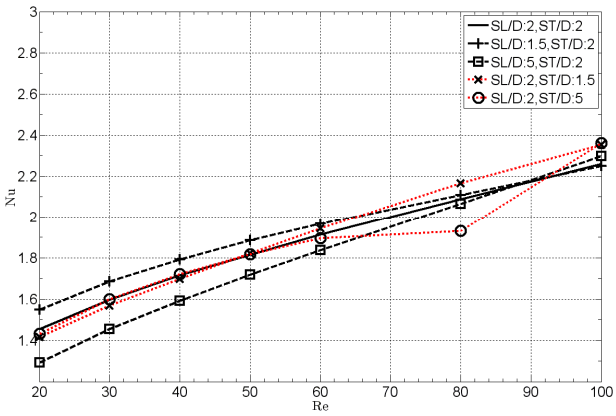

Figure 18: *H*/*D*=4, Nu vs Re

4 CONCLUSION

In this numerical work, first, an experimentally tested device was modeled, and then, numerical heat transfer results were obtained. The results were compared to experimental data to show the credibility of numerical models. Following that, a geometrically repetitive pattern from a typical micro pin-fin heat sink was chosen and became the base of parametric runs. In these runs, the repetitive pattern always contained the same amount of micro pin fins. However, the channel dimension varied to surrender the occupied area defined by varying *SL*, *ST* and *D* values. Therefore, this parametric optimization is independent of predicting the performance of a heat sink with a

varying density of pin-fins at a fixed micro channel geometry. The results show that:

- *SL*/*D* and *ST*/*D* have negative and positive effects on friction factor independent of *H*/*D* and Re, respectively.
- For *H*/*D*=0.5, *SL*/*D* and *ST*/*D* affect Nusselt number in parallel lines with friction factor.
- For higher *H*/*D* the trends in Nu become complex and highly dependent on working conditions (Re) and H/D ratio.

ACKNOWLEDGEMENTS

This work was supported by Sabanci University Internal Research Grant, no: IACF09-00642. Graduate student support provided by the Faculty of Engineering and Natural Sciences of Sabanci University is greatly appreciated. The authors thank to Prof. Kürşat Şendur for his help in the assessment of the workstations in the Mechatronics Systems Laboratory, Sabanci University.

REFERENCES

[1] Tuckerman, D. B., and Pease, R. F. W., 1981, "High-Performance Heat Sinking for VLSI," *IEEE Electron Device Lett.*, **2**, pp. 126–129.

[2] Phillips, R. J., 1990, "Micro-Channel Heat Sinks," *Advances in Thermal Modeling of Electronic Components*, A. Bar-Cohen, and A. D. Kraus eds., ASME, New York, **2**, pp. 109–184.

[3] Knight, R. W., Hall, D. J., Goodling, J. S., and Jaeger, R. C., 1992, "Heat Sink Optimization with Application to Microchannels," *IEEE Trans. Compon., Hybrids, Manuf. Technol.*, **15**, pp. 832–842.

[4] Harms, T. M., Kazmierczak, M. J., and Cerner, F. M., 1999, "Developing Convective Heat Transfer in Deep Rectangular Microchannels," *Int. J. Heat Fluid Flow*, **20**, pp. 149–157.

[5] Fedorov, A. G., and Viskanta, R., 2000, "Three-Dimensional Conjugate Heat Transfer in the Microchannel Heat Sink for Electronic Packaging," *Int. J. Heat Mass Transfer*, **43**, pp. 399–415.

[6] Qu, W., and Mudawar, I., 2002, "Analysis of Three-Dimensional Heat Transfer in Micro-Channel Heat Sinks," *Int. J. Heat Mass Transfer*, **45**, pp. 3973–3985.

[7] Qu, W., and Mudawar, I., 2002, "Experimental and Numerical Study of Pressure Drop and Heat Transfer in a Single-Phase Micro-Channel Heat Sink," *Int. J. Heat Mass Transfer*, **45**, pp. 2549–2565.

[8] Li, J., Peterson, G. P., and Cheng, P., 2004, "Three-Dimensional Analysis of Heat Transfer in a Micro-Heat Sink with Single Phase Flow," *Int. J. Heat Mass Transfer*, **47**, pp. 4215–4231.

[9] Lee, P. S., Garimella, S. V., and Liu, D., 2005, "Investigation of Heat Transfer in Rectangular Microchannels," *Int. J. Heat Mass Transfer*, **48**, pp. 1688–1704.

[10] Jasperson, B. A., Jeon, Y., Turner, K. T., Pfefferkorn, F. E. and Qu, W., 2010, "Comparison of Micro-Pin-Fin and Microchannel Heat Sinks Considering Thermal-Hydraulic Performance and Manufacurability," *IEEE Trans. Comp. and Pack. Tech.*, **33**, pp. 148-160.

[11] Wong, M., Owen, I., Sutcliffe, C.J. and Puri, A., 2009, "Convective heat transfer and pressure losses across novel heat sinks fabricated by Selective Laser Melting", *Int. J. Heat and Mass Transfer*, ***52***, pp. 281-288.

[12] Peles, Y., Kosar, A., Mishra, C., Kuo, C.-J., and Schneider, B., 2005, "Forced Convective Heat Transfer Across a Pin Fin Micro Heat Sink," *Int. J. Heat Mass Transfer*, **48**, pp. 3615–3627.

[13] Kosar, A., and Peles, Y., 2006, "Thermal-Hydraulic Performance of MEMSBased Pin Fin Heat Sink," *ASME J. Heat Transfer*, **128**, pp. 121–131.

[12] Short, B. E., Jr., Raad, P. E., and Price, D. C., 2002, "Performance of Pin Fin Cast Aluminum Coldwalls, Part 1: Friction Factor Correlation," *J. Thermophys. Heat Transfer*, **16**, pp. 389–396.

[13] Short, B. E., Jr., Raad, P. E., and Price, D. C., 2002, "Performance of Pin Fin Cast Aluminum Coldwalls, Part 2: Colburn j-Factor Correlations," *J. Thermophys. Heat Transfer*, **16**, pp. 397–403.

[14] Moores, K. A., and Joshi, Y. K., 2003, "Effect of Tip Clearance on the Thermal and Hydrodynamic Performance of a Shrouded Pin Fin Array," *ASME J. Heat Transfer*, **125**, pp. 999–1006.

[15] Kosar, A., Mishra, C., and Peles, Y., 2005, "Laminar Flow across a Bank of Low Aspect Ratio Micro Pin Fins," *ASME J. Fluids Eng.*, **127**, pp. 419–430.

[16] Kosar, A., Kuo, C., and Peles, Y., 2006, "Hydoroil-Based Micro Pin Fin Heat Sink," *Proceeding of IMECE 2006*, Paper No. IMECE2006-13257.

[17] Hu-Sio, A., Qu, W., 2007, "Experimental Study of Pressure Drop and Heat Transfer in a Single Phase Micropin-Fin Heat Sink" *ASME Journal of Electronics Packaging*, **129**, pp.479-487

[18] Kosar, A. and Peles, Y., 2007, "Micro Scale Pin Fin Heat Sinks-Parametric Performance Evaluation Study" *IEEE Trans. Comp. and Pack. Tech.*, **30**, no: 4, pp. 855-865.

[19] Kosar, A., Peles, Y., 2006, "Convective flow of refrigerant (R-123) across a bank of micro pin fins", *Int. J. Heat and Mass Transfer*, **49**, pp. 3142-3155.

[20] Hu-Sio, A., Qu, W., 2008, "Liquid Single-Phase Flow in an Array of Micro-Pin-Fins – Part I: Heat Transfer Characteristics" *ASME J. of Heat Transfer*, **130**, pp.122402-1 – 122402-11.

[21] Hu-Sio, A., Qu, W., 2008, "Liquid Single-Phase Flow in an Array of Micro-Pin-Fins – Part II: Pressure Drop Characteristics" *ASME J. of Heat Transfer*, **130**, pp.122405-1 – 122405-4.